

# Water-Powered Cell-Mimicking Janus Micromotor

Zhiguang Wu, Jinxing Li, Berta Esteban-Fernández de Ávila, Tianlong Li, Weiwei Gao, Qiang He, Liangfang Zhang,\* and Joseph Wang\*

**Cell derivatives have received increasing attention due to their unique ability to mimic many of the natural properties displayed by their source cells. Integration of cell-derived natural materials with synthetic subjects can be applied toward the development of novel biomedical nano/microscale devices for a wide range of applications, including drug delivery and biodetoxification. Herein, a cell membrane functionalized magnesium-based Janus micromotor, powered by water, that mimics natural motile cells is reported. The new cell-mimicking Janus micromotor is constructed by integrating red blood cell (RBC) membranes, gold nanoparticles (AuNPs), and alginate (ALG) onto the exposed surface areas of magnesium microparticles that are partially embedded in Parafilm. The resulting RBC membrane-coated magnesium (RBC-Mg) Janus micromotors display an efficient and guided propulsion in water without any external fuel, as well as in biological (albumin-rich) media with no apparent biofouling, mimicking the movement of natural motile cells. The effective RBC membrane coating bestows the RBC-Mg Janus micromotors with unique capability for absorbing and neutralizing both biological protein toxins and nerve agent simulants. Such detoxification ability is facilitated greatly by the water-driven motion of the motors. The RBC-Mg Janus micromotors represent an exciting progress toward cell-mimicking microscale motors that hold great promise for diverse biomedical and biodefense applications.**

## 1. Introduction

Nature has been a constant source of inspiration for scientists and engineers to design and develop synthetic structures that mimic the complexity and functionalities of biological systems. The fabrication of versatile artificial micro/nanomotors, possessing advanced mobility and biological functions, represents an exciting yet challenging task in the field of nanobiotechnology.<sup>[1–12]</sup> The autonomous movement found in

living cells, such as neutrophile granulocytes,<sup>[13,14]</sup> has stimulated considerable interest in developing chemically powered synthetic motors that mimic the behavior of natural cells to achieve various complex functions.<sup>[15–19]</sup> For these synthetic motors, their chemical propulsion has commonly relied on different types of fuels, including hydrogen peroxide,<sup>[20–26]</sup> hydrazine,<sup>[27]</sup> strong acids or bases,<sup>[28–30]</sup> and bromine/iodine.<sup>[31]</sup> Considerable recent attention has been given to water-powered magnesium-based motors since water represents the ideal fuel for most practical applications of synthetic micro/nanomotors.<sup>[32–35]</sup> To implement sophisticated functionalities onto synthetic subjects, new biomimetic systems that harness natural cell functions have been introduced recently, as was demonstrated by coating synthetic nanoparticles with cell membrane derived directly from natural cells.<sup>[36,37]</sup> These biomimetic particles have demonstrated impressive potential applications, ranging from systemic drug delivery to removal of toxins and to effective vaccine development.<sup>[38–40]</sup> These recent advances suggest that integrating cell membranes to synthetic micro/nanomotors may bestow some unprecedented properties to the motors that are otherwise difficult to achieve with purely synthetic motors.

The objective of the present work is to develop and characterize a red blood cell (RBC) membrane-functionalized magnesium-based (RBC-Mg) Janus micromotor that is powered solely by water. The biomimetic RBC-Mg Janus motors are prepared by selectively assembling RBC membranes onto one side of Mg particles using the parafilm method. The self-propulsion of the motors is based on the spontaneous Mg–water reaction that produces hydrogen bubbles. The unique functions and advantages of the RBC-Mg Janus motors are demonstrated in operation in protein-rich biological media and detoxification protocols using model protein toxins and chemical warfare agents. The cell-mimicking RBC-Mg Janus motor thus acts as decoy to attract, capture, and neutralize toxins in biological fluids. In addition, the materials of the RBC-Mg motor, including magnesium, chitosan, gold nanoparticles, and alginate, along with the Mg<sup>2+</sup> byproduct, are well known to be biocompatible, indicating that the RBC-Mg Janus motor will not cause adverse or toxic effects. The results testify the advanced functions and robustness of the new water-powered RBC-Mg micromotors, which

Dr. Z. Wu, J. Li, Dr. B. E.-F. de Ávila,  
T. Li, Dr. W. Gao, Prof. L. Zhang, Prof. J. Wang  
Department of Nanoengineering  
University of California  
San Diego, La Jolla, CA 92093, USA  
E-mail: zhang@ucsd.edu;  
josephwang@ucsd.edu

Dr. Z. Wu, T. Li, Prof. Q. He  
Key Lab for Microsystems and Microstructure Manufacturing  
Harbin Institute of Technology  
Harbin 150080, P.R. China

DOI: 10.1002/adfm.201503441



hold considerable promise for a number of practical biomedical applications.

## 2. Results and Discussion

The fabrication process of the RBC-Mg Janus micromotors is schematically illustrated in **Figure 1A**. In the first step, a layer of Mg particles with a diameter of 10–20  $\mu\text{m}$  was dispersed onto a Parafilm-coated glass slide. Upon the spray coating, the Mg particles were partially embedded into the Parafilm and the remaining area of the particles was exposed for subsequent fabrication processes. This would result in an asymmetric motor structure, namely Janus motor. Specifically, the Parafilm (containing the embedded Mg particles) was consecutively immersed into a chitosan-stabilized gold nanoparticles (AuNPs) solution and an alginate (ALG) solution. The AuNPs (diameter: 30–60 nm), which are responsible for efficient propulsion by performing a macrogalvanic corrosion of the oxide passivation layer on the Mg surface,<sup>[32]</sup> possess a high surface tension and thus intend to adsorb onto the Mg particles to minimize the system's free energy. A negatively charged ALG layer was subsequently assembled onto the positively charged AuNPs surface, forming the shell coating of the Mg motors. Next,

preformed RBC membrane-derived vesicles (diameter: 50–100 nm) were added to the system, to fuse onto the outer ALG surface layer. The negatively charged ALG layer favors the interaction with the less negative cytoplasmic side of the RBC membrane, resulting in a thin RBC membrane coating with a right-side-out orientation on the AuNP/ALG-covered Mg particles. Finally, well-separated RBC-Mg Janus motors were obtained after partial dissolution of the Parafilm in tetrahydrofuran. Note that tetrahydrofuran may cause negligible adverse effect on the membrane proteins,<sup>[41]</sup> indicating that the function of natural RBC membrane is well preserved on the RBC-Mg Janus motors. The resulting RBC-Mg Janus motors were stable in HEPES buffer solution (pH 8.5), where the magnesium particles are not dissolved and the functional biomolecules (mainly proteins) are stable under weak alkaline conditions. The RBC-Mg motors have high dispersity in aqueous media, with the high negative charge of the RBC membrane preventing aggregation of the particles by electrostatic repulsion.

The scanning electron microscopy (SEM) image in **Figure 1B** displays the resulting RBC-Mg Janus motor with spherical geometry ( $\approx 20 \mu\text{m}$ ) and a small circular opening ( $\approx 2 \mu\text{m}$ ). The small hole is attributed to the portion of the surface of the Mg particles embedded in the Parafilm during their coating with the RBC/AuNP/ALG layer. Fluorescently labeled RBC membranes

were employed to verify the successful coating of the motors with the cell membranes. A red fluorescence is clearly observed on the outer surface of the RBC-Mg Janus motor in Rhodamine B (RhB) channel (Figure 1C). Importantly, no fluorescence signal is observed from the opening area of the motor, indicating successful coating of the RBC membranes only on the exposed portion of the Mg particles, which resulted in the formation of asymmetric RBC-Mg Janus motors. In addition, because of the nature of layer-by-layer technique, the RBC content in the resulting coating can be tuned by sequential assembly of the alginate and RBC vesicle layers.

The highly efficient locomotion of the RBC-Mg Janus motors involves the bubble propulsion mechanism which utilizes hydrogen bubbles produced from the spontaneous redox reaction of Mg and water (**Figure 2A**). The macrogalvanic corrosion of the RBC-Mg Janus motors with AuNPs and pitting corrosion of coexisting chloride ions result in efficient formation of hydrogen bubbles, which is essential for the continuous propulsion of the motors.<sup>[32,42]</sup> **Figure 2B** shows a microscopy image, captured from Video S1 (Supporting Information), corresponding to the random movement of an RBC-Mg Janus motor in a 0.08 M NaCl solution. It could be clearly observed that the generation, growth, and detachment of hydrogen bubbles occurred on the opening hole of the RBC-Mg Janus motor. The track line displayed the motion of the RBC-Mg Janus

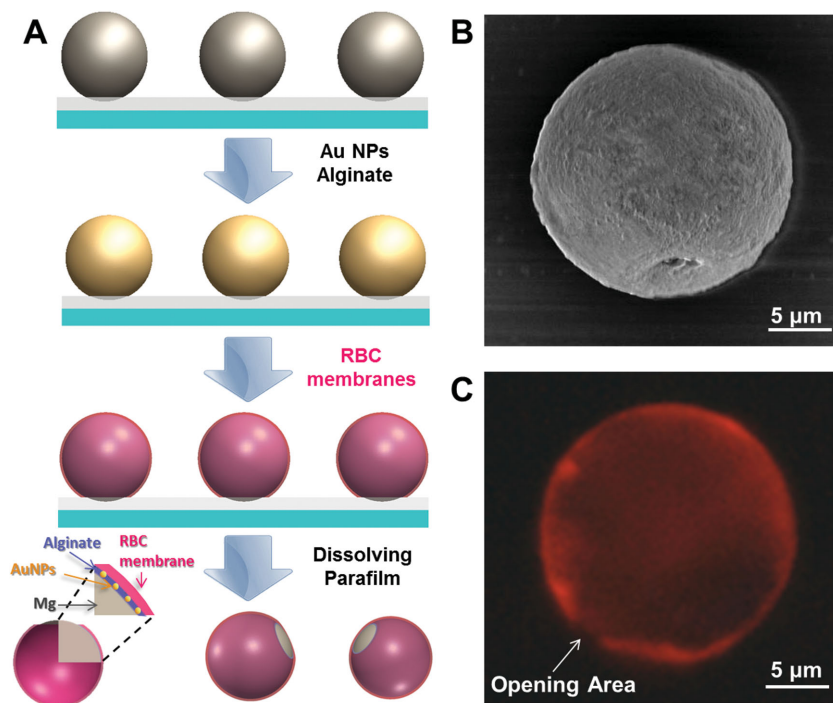


**Figure 1.** Preparation and characterization of RBC membrane-coated magnesium (RBC-Mg) Janus micromotor. A) Scheme of the fabrication process of the RBC-Mg Janus micromotor. From top to bottom: 1) a layer of Mg particles is dispersed onto Parafilm and the particles are then partially embedded in the Parafilm; 2) deposition of gold nanoparticles (AuNPs) and alginate (ALG) onto the exposed surface of the Mg particles; 3) coating of RBC membrane onto the AuNP/ALG-covered surface of the Mg particles; and 4) releasing the RBC-Mg Janus micromotor by dissolution of Parafilm in tetrahydrofuran (the inset image shows the cross-section of the RBC-Mg Janus micromotor). B) SEM image of a representative RBC-Mg Janus micromotor. C) Fluorescence image of a representative RBC-Mg Janus micromotor, in which the RBC membrane is labeled with Rhodamine B (RhB).

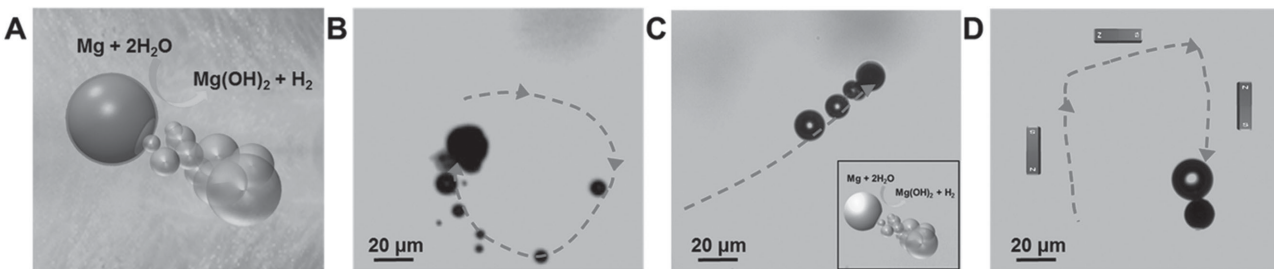


**Figure 2.** Movement of RBC-Mg Janus micromotor in water containing 0.08 M NaCl. A) Schematic illustration of the motion mechanism of the RBC-Mg Janus micromotor. B) Random motion of a RBC-Mg Janus micromotor. C) Random motion of a Mg micromotor without the RBC membrane coating. D) Magnetically guided motion of a  $\text{Fe}_3\text{O}_4$ -loaded RBC-Mg Janus micromotor (arrows indicate the direction of the motion).

motor over a 2 s period, with an average speed of  $172 \mu\text{m s}^{-1}$ . The drag force of the micromotor was estimated to be 2 pN by using the Stokes drag theory. Bare Mg Janus motor (without RBC membrane coating) displayed similar movement with negligible change of speed ( $165 \mu\text{m s}^{-1}$ ) under the same experimental conditions (Figure 2C), indicating that the RBC-membrane coverage had a negligible effect upon the reaction of Mg and water and hence propulsion efficiency.

Controlled movement of the RBC-Mg Janus motor can be achieved through the incorporation of additional negatively charged  $\text{Fe}_3\text{O}_4$  nanoparticles into the multilayered coating of the motor *via* electrostatic attraction (see Experimental Section in the Supporting Information). As shown in Figure 2D and the corresponding Video S1 (Supporting Information), the resulting  $\text{Fe}_3\text{O}_4$ -loaded RBC-Mg Janus motor can be navigated precisely along predefined trajectories under external magnetic guidance. A “U” turn trajectory of the RBC-Mg motor can thus be observed while the motor is moving at speed of  $160 \mu\text{m s}^{-1}$ . Such magnetically guided motion of RBC-Mg Janus motor holds considerable promise for biomedical applications of the motors, for instance, cancer cell isolation, targeted drug delivery, or removal of toxins (which will be discussed below).

One important feature of the RBC-Mg Janus motor lies in its antifouling capability that facilitates efficient propulsion in biological fluids. The RBC membrane coverage shields the motor from protein fouling effects when subjected to biological fluids, taking advantage of the antifouling property of RBCs (Figure 3Aa). Figure 3Ab shows the efficient movement of the RBC-Mg motor in albumin-rich medium with a speed of  $33 \mu\text{m s}^{-1}$ . While this speed is lower than the  $172 \mu\text{m s}^{-1}$  observed in water (due to the increased viscosity of the solution), such propulsion is sufficient for conducting various tasks in biological environments. In contrast, severe protein fouling rapidly occurs on the surface of the bare Mg motor (without RBC membrane coating), dramatically hindering the Mg–water reaction, the generation of hydrogen bubbles and thus the propulsion

efficiency (Figure 3Ba,b). The corresponding Video S2 (Supporting Information) shows the minor bubble formation, with no directional propulsion of the bare Mg Janus motor in the albumin solution.

Further, we demonstrated that the function of cell-mimicking RBC-Mg Janus motors as a decoy to attract, capture, and neutralize toxins in biological fluids, while the RBC membrane surface prevents nonspecific adsorption of common plasma proteins. To examine the detoxification capability of the RBC-Mg Janus motors, we selected a well-documented cell membrane-damaging toxin,  $\alpha$ -toxin, and mixed it with the RBC-Mg Janus motors in a 5% albumin solution. The detoxification capability of the RBC-Mg Janus motors for absorbing and neutralizing the  $\alpha$ -toxin are achieved by camouflaging natural red blood cells. Such RBC-camouflaging Janus motor can be used as

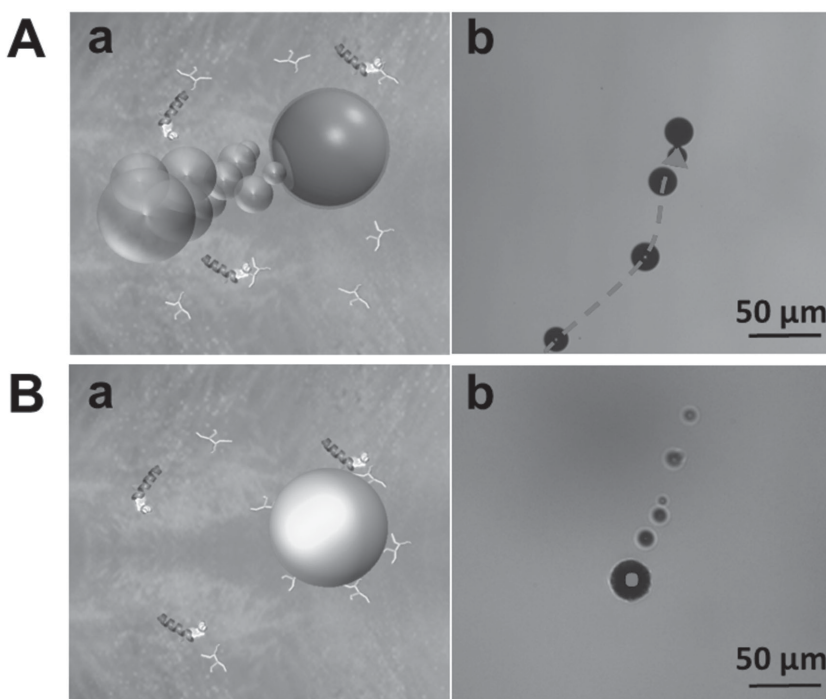


**Figure 3.** Movement of RBC-Mg Janus micromotor in biological fluid. a) Schematic illustrations of the movement in albumin-rich media of A) a RBC-Mg Janus micromotor and B) a Mg micromotor without RBC membrane coating. b) Microscopy images showing the motion of A) a RBC-Mg Janus micromotor and B) a Mg micromotor without RBC membrane coating over a 5 s period. Media: 5 wt% albumin aqueous solution containing 0.08 M NaCl.

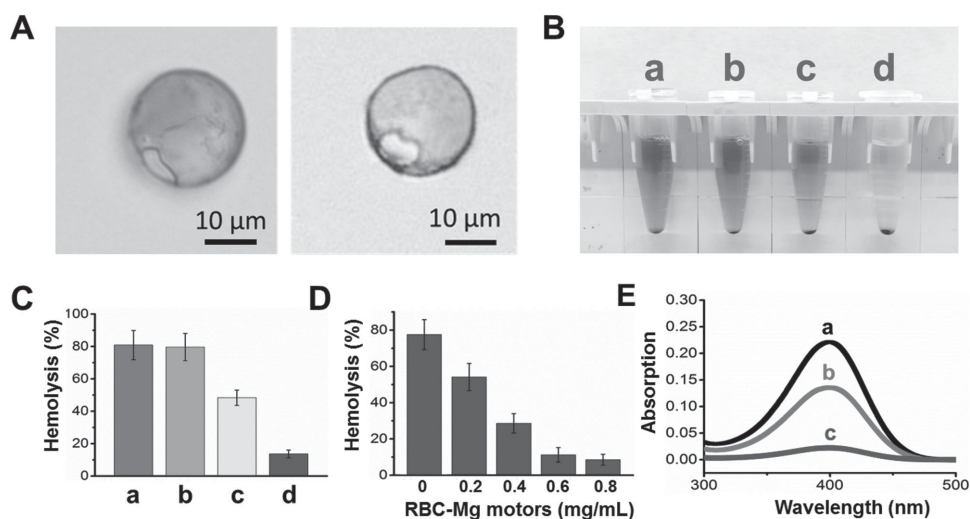


**Figure 4.** Detoxification test of RBC-Mg Janus micromotors. A) Microscopy images showing a complete, hollow shell structure of a RBC-Mg Janus micromotor after complete dissolution of the Mg core in the absence (left) and presence (right) of  $\alpha$ -toxin. B) Images of centrifuged RBCs after incubation with  $\alpha$ -toxin/albumin mixture solution in a) PBS, b) AuNP/ALG-covered Mg micromotor (without RBC membrane), c) RBC membrane-coated silica microparticles (RBC-SiO<sub>2</sub>), and d) RBC-Mg Janus micromotors. C) Hemolysis quantification of samples shown in (B). D) Hemolysis quantification of  $\alpha$ -toxin and albumin solution in the presence of different concentrations of RBC-Mg Janus micromotors. E) Absorbance spectra of methyl paraoxon after 5 min incubation with different samples: a) PBS, b) 1.5 mg mL<sup>-1</sup> of RBC-SiO<sub>2</sub>, and c) 1.5 mg mL<sup>-1</sup> of RBC-Mg Janus micromotors. Error bars represent standard deviations.

decoys to absorb and neutralize the toxin. Similar to the propulsion observed in albumin solution, the RBC-Mg Janus motor displayed a random motion in the  $\alpha$ -toxin/albumin solution, preserving a hollow shell structure after the Mg core was completely dissolved (Figure 4A). Such structure was able to retain the absorbed  $\alpha$ -toxin and neutralize its virulence, thereby, protecting cells from damaging by the toxins. Equal amounts of PBS buffer, bare Mg motors (without RBC membrane coating), and RBC membrane-coated SiO<sub>2</sub> particles (without movement), were employed as controls and tested in parallel to the RBC-Mg Janus motors by incubating with the  $\alpha$ -toxin for 5 min followed by adding 1.5 mL of 2 vol% RBCs to each formulation. As shown in Figure 4B, the incubation of  $\alpha$ -toxin and RBC-Mg Janus motors resulted in a clean supernatant compared to the control groups, indicating the effectiveness of the coated RBC membranes in absorbing toxins and the importance of the motor propulsion in accelerating the detoxification process. The detoxification efficiency was further quantified by measuring the absorption of the released hemoglobin (540 nm), defined as relative hemolysis (Figure 4C). The treatment of bare Mg Janus motors displayed a negligible decrease of the relative hemolysis as compared with the treatment of PBS. This was likely attributed to the absence of RBC membranes and the albumin fouling effect on the bare motors, which might block the nonspecific adsorption of  $\alpha$ -toxin onto the motors. In contrast, a sharp decrease of relative hemolysis down to 48% and 9% was observed in samples treated with RBC-coated SiO<sub>2</sub> particles and RBC-Mg Janus motors, respectively. The comparison between the treatment with RBC-Mg Janus motors and RBC-coated SiO<sub>2</sub> particles shows that the water-powered propulsion significantly enhanced the detoxification efficiency. Moreover, a higher detoxification capacity was achieved by increasing the concentration of RBC-Mg motors over the range of 0–0.8 mg mL<sup>-1</sup>, showing that the relative hemolysis decreased from 78%

without RBC-Mg Janus motors to 9% using motor concentration of 0.8 mg mL<sup>-1</sup> (Figure 4D).

To expand the potential detoxification of the RBC-Mg motor toward diverse environmental remediation, we further tested its decontamination ability against a nerve agent simulant, methyl-paraoxon, in albumin solution. Organophosphorus agents are known to interact with RBC and to inhibit the acetylcholinesterase on RBC membranes.<sup>[43]</sup> Thus, the acetylcholinesterase presents in the RBC membranes of the magnesium motor, is able to absorb and remove the paraoxon. The UV-vis absorbance spectra in Figure 4E shows that RBC-Mg motors were able to reduce the level of the nerve agent simulant by 90.0% as compared to the PBS sample, while the corresponding nonmotor RBC-SiO<sub>2</sub> particles neutralized about 38.2% of the agent. Apparently, the water-driven motion of the RBC membrane coating improves the speed of the decontamination process.

### 3. Conclusions

We have presented the first example of cell-mimicking water-powered micromotors based on cell membrane-coated magnesium microparticles. The bioinspired motors were prepared by the assembly of RBC membranes onto magnesium particles, resulting in efficient propulsion in water and biological media without the need for external fuels or fields. The cell membrane coating shielded the motor from protein fouling effects when the motors are operated in a biological fluid. The resulting cell-mimicking RBC-Mg Janus motors act as decoys that attract and neutralize toxins. The potential application of the RBC-Mg motors has been demonstrated toward rapid detoxification of  $\alpha$ -toxin and methyl-paraoxon, models of membrane-damaging toxins and chemical warfare agents, respectively. The same synthesis procedure could be extended to various other types of cell membranes,

which makes these biomimetic Janus motors appealing for a broad range of biomedical and biodefense applications.

## Supporting Information

Supporting Information is available from the Wiley Online Library or from the author.

## Acknowledgments

Z.W., J.L., and B. E-F.A. contributed equally to this work. This project received support from the Defense Threat Reduction Agency Joint Science and Technology Office for Chemical and Biological Defense (Grant Nos. HDTRA1-13-1-0002 and HDTRA1-14-1-0064). Z.W. and T.L. have been supported by the Scholarship Fund from China Scholarship Council (CSC).

Received: August 15, 2015

Revised: September 24, 2015

Published online: November 9, 2015

- [1] J. Wang, *Nanomachines: Fundamentals and Applications*, Wiley-VCH, Weinheim, Germany 2013.
- [2] Y. Mei, A. A. Solovev, S. Sanchez, O. G. Schmidt, *Chem. Soc. Rev.* **2011**, *40*, 2109.
- [3] G. A. Ozin, I. Manners, S. Fournier-Bidoz, A. Arsenault, *Adv. Mater.* **2005**, *17*, 3011.
- [4] T. E. Mallouk, A. Sen, *Sci. Am.* **2009**, *300*, 72.
- [5] H. Wang, M. Pumera, *Chem. Rev.* **2015**, *115*, 8704.
- [6] S. Sánchez, L. Soler, J. Katuri, *Angew. Chem. Int. Ed.* **2015**, *54*, 1414.
- [7] G. Loget, A. Kuhn, *Nat. Commun.* **2011**, *2*, 535.
- [8] L. Li, J. Wang, T. Li, W. Song, G. Zhang, *Soft Matter* **2014**, *10*, 7511.
- [9] A. Ghosh, P. Fischer, *Nano Lett.* **2009**, *9*, 2243.
- [10] D. A. Wilson, R. J. M. Nolte, J. C. M. van Hest, *Nat. Chem.* **2012**, *4*, 268.
- [11] D. Schamel, A. G. Mark, J. G. Gibbs, C. Miksch, K. I. Morozov, A. M. Leshansky, P. Fischer, *ACS Nano* **2014**, *8*, 8794.
- [12] T. Xu, F. Soto, W. Gao, R. Dong, V. Garcia-Gradilla, E. Magaña, X. Zhang, J. Wang, *J. Am. Chem. Soc.* **2015**, *137*, 2163.
- [13] D. Metcalf, *Science* **1985**, *229*, 16.
- [14] E. Kolaczkowska, P. Kubes, *Nat. Rev. Immunol.* **2013**, *13*, 159.
- [15] J. Wang, *ACS Nano* **2009**, *3*, 4.
- [16] V. Magdanz, S. Sanchez, O. G. Schmidt, *Adv. Mater.* **2013**, *25*, 6581.
- [17] M. Guix, C. C. Mayorga-Martinez, A. Merkoçi, *Chem. Rev.* **2014**, *114*, 6285.
- [18] P. G. van Rhee, R. S. M. Rikken, L. K. E. A. Abdelmohsen, J. C. Maan, R. J. M. Nolte, J. C. M. van Hest, P. C. M. Christianen, D. A. Wilson, *Nat. Commun.* **2014**, *5*, 5010.
- [19] T. Xu, F. Soto, W. Gao, V. Garcia-Gradilla, J. Li, X. Zhang, J. Wang, *J. Am. Chem. Soc.* **2014**, *136*, 8552.
- [20] J. Li, W. Gao, R. Dong, A. Pei, S. Sattayasamitsathit, J. Wang, *Nat. Commun.* **2014**, *5*, 5026.
- [21] L. Li, J. Wang, T. Li, W. Song, G. Zhang, *J. Appl. Phys.* **2015**, *117*, 104308.
- [22] Z. Wu, Y. Wu, W. He, X. Lin, J. Sun, Q. He, *Angew. Chem. Int. Ed.* **2013**, *52*, 7000.
- [23] X. Ma, K. Hahn, S. Sanchez, *J. Am. Chem. Soc.* **2015**, *137*, 4976.
- [24] H. Wang, J. G. S. Moo, M. Pumera, *Nanoscale* **2014**, *6*, 11359.
- [25] Z. Wu, X. Lin, Y. Wu, T. Si, J. Sun, Q. He, *ACS Nano* **2014**, *8*, 6097.
- [26] H. Wang, G. Zhao, M. Pumera, *J. Am. Chem. Soc.* **2014**, *136*, 2719.
- [27] W. Gao, A. Pei, R. Dong, J. Wang, *J. Am. Chem. Soc.* **2014**, *136*, 2276.
- [28] W. Gao, M. D'Agostino, V. Garcia-Gradilla, J. Orozco, J. Wang, *Small* **2013**, *9*, 467.
- [29] W. Gao, A. Uygun, J. Wang, *J. Am. Chem. Soc.* **2012**, *134*, 897.
- [30] W. Gao, R. Dong, S. Thamphiwatana, J. Li, W. Gao, L. Zhang, J. Wang, *ACS Nano* **2015**, *9*, 1117.
- [31] S. Sengupta, M. E. Ibele, A. Sen, *Angew. Chem. Int. Ed.* **2012**, *51*, 8434.
- [32] W. Gao, X. Feng, A. Pei, Y. Gu, J. Li, J. Wang, *Nanoscale* **2013**, *5*, 4696.
- [33] W. Gao, A. Pei, J. Wang, *ACS Nano* **2012**, *6*, 8432.
- [34] J. Li, V. V. Singh, S. Sattayasamitsathit, J. Orozco, K. Kaufmann, R. Dong, W. Gao, B. Jurado-Sánchez, Y. Fedorak, J. Wang, *ACS Nano* **2014**, *8*, 11118.
- [35] F. Mou, C. Chen, H. Ma, Y. Yin, Q. Wu, J. Guan, *Angew. Chem. Int. Ed.* **2013**, *52*, 7208.
- [36] C.-M. J. Hu, L. Zhang, S. Aryal, C. Cheung, R. H. Fang, L. Zhang, *Proc. Natl. Acad. Sci. USA* **2011**, *108*, 10980.
- [37] W. Gao, C.-M. J. Hu, R. H. Fang, B. T. Luk, J. Su, L. Zhang, *Adv. Mater.* **2013**, *25*, 3549.
- [38] Z. Wu, T. Li, W. Gao, T. Xu, Dr. B. Jurado-Sánchez, J. Li, W. Gao, L. Zhang, J. Wang, *Adv. Funct. Mater.* **2015**, *25*, 3881.
- [39] C.-M. J. Hu, R. H. Fang, J. Copp, B. T. Luk, L. Zhang, *Nat. Nanotechnol.* **2013**, *8*, 336.
- [40] C.-M. J. Hu, R. H. Fang, B. T. Luk, L. Zhang, *Nat. Nanotechnol.* **2013**, *8*, 933.
- [41] K. Griebelow, A. M. Klibanov, *J. Am. Chem. Soc.* **1996**, *118*, 11695.
- [42] G. Song, A. Atrens, *Adv. Eng. Mater.* **2003**, *5*, 837.
- [43] M. Eddlestona, N. A. Buckley, Peter Eyer, A. H. Dawson, *The Lancet* **2008**, *371*, 597.